2023

AC Ground Fault Location for DC–AC Inverters Based on a Grounding Resistor Voltage Analysis

JOSÉ M. GUERRERO, GUSTAVO NAVARRO, AND CARLOS A. PLATERO

This is an “Accepted article” version of a paper and it is not the “Final published article” version as appearing in IEEE Transactions on Industry Applications (Volume: 58, Issue: 3, May-June 2022) and published on 22 February 2022.

How to Cite this article:

J. M. Guerrero, G. Navarro and C. A. Platero, "AC Ground Fault Location for DC–AC Inverters Based on a Grounding Resistor Voltage Analysis," in *IEEE Transactions on Industry Applications*, vol. 58, no. 3, pp. 3613-3623, May-June 2022, doi: 10.1109/TIA.2022.3152683.

DOI: https://doi.org/10.1109/TIA.2022.3152683

AC Ground Fault Location for DC-AC Inverters Based on a Grounding Resistor Voltage Analysis

José M. Guerrero, Gustavo Navarro, and Carlos A. Platero, *Senior Member, IEEE*

***Abstract*—Ground fault diagnosis is difficult to carry out in DC-AC systems due to the presence of power electronics. Additionally, it is common that neither relays could protect efficiently these systems as AC devices are not prepared to actuate under DC currents and vice versa. Previous studies were able to detect if the fault was in AC or DC but the faulty point still being incognita. This paper presents a ground fault location method for the AC side of DC-AC systems that complements previous detection methods. It is based on a grounding resistor placed in the midpoint of the DC bus. Then, an instantaneous voltage window record is analyzed into a histogram, obtaining two representative voltage peaks that are correlated. These values are the one with most repetitions and the one with most amplitude. Attending to a coefficient defined by these two parameters, the fault location can be estimated. The effectiveness of this method has been corroborated with simulations and experimental tests in a 140 kW converter, achieving promising results.**

***Index Terms*—AC-DC power converters, Fault diagnosis, Fault location, Ground fault, Statistical analysis, Voltage measurement.**

I. Introduction

NOWADAYS, most of the electric drives are controlled and monitored to increase their efficiency [1]-[2]. This can be achieved thank to power converters, which allow the variation of the electrical conditions such as current [3], voltage [4], or frequency [5]-[6].

DC-AC system topologies are used for example in electric vehicles (EVs), where the DC bus is composed by batteries which feed the AC side, controlled by an inverter, where there are one or more electric motors [7]-[8].

However, the fault detection, protection and location are difficult for these DC-AC systems [9]. Ground faults are the most typical type of electrical failure in power systems [10]-[11]. They are mainly produced by the lack of insulation between an active part and ground. In this case a fast detection is needed [9] before a second ground fault appears and it will lead into a phase-to-phase fault. This way, ground fault diagnosing is a very active research field in power systems, e.g., in ungrounded DC systems [12], traction power systems [13], synchronous machines [14]-[15] or distribution systems [16] among others.

To protect electric systems against ground faults, a huge variety of ground fault detectors, locators and protections have been developed. Most of the electric systems are grounded. Then, in case of ground fault, there is a fault current circulating between the grounded point and the fault. The value of the grounding impedance usually limits the fault current. In case of isolated systems, the detection is normally performed by voltages measurement. Focusing on grounded systems, the operating principles and devices for ground fault diagnosis are diverse.

A. *Ground overcurrent protection (51N)*

It registers the current which circulates though a neutral point of the circuit, as it can be the neutral of a synchronous generator. If fault current is higher than a certain threshold, the protection equipment will trip. In low voltage systems as photovoltaics also, fuses can be used [17].

B. *Neutral over voltage protection (59N)*

It registers the voltage between a neutral point and ground by placing a grounding resistor between these points and measuring in its terminals. If the voltage value is over a certain threshold, the protection emits the trip and alarm signals to the corresponding breaker. In case of large electric generators, this protection is combined with others in order to protect the whole windings of the machine, it is known as 100% stator ground fault protection [18]-[19]. In this field, more advanced techniques propose using the neutral voltage measurement combined with AC phase voltages and DC voltage to locate ground faults in rotors of synchronous machines with static excitation [20].

C. *Neutral differential protection (87N)*

Many possibilities can be used with differential principle. One of them, to detect ground faults, on the comparison of the zero sequence currents at both ending of an electrical element, as lines or generators [21]. This method could also work for adjustable speed drives where the current transformers include the three phase cables, but it could experience saturation in case of DC faults [22].

D. *Under-impedance relay (21)*

This type of protection needs the phase currents and voltages. Using these measurements, the protection calculates the impedance in real time dividing the voltage between current in each each phase. In case of ground fault, if a calculated phase impedance is lower than a certain adjustable value, it means the presence of a fault in this phase [23].

This work was supported in part by the Universidad Politécnica de Madrid and part by the Centro de Investigaciones Energéticas, Medioambientales y Tecnológicas (CIEMAT) of Spain.

J.M. Guerrero is with the Energy and Fuels Department, ETSIME, Universidad Politécnica de Madrid, Madrid 28003 (Spain). E-mail: josemanuel.guerrero@upm.es

C.A. Platero is with the Automatic, Electric and Electronic and Industrial Computing Department, ETSII, Universidad Politécnica de Madrid, Madrid 28006 (Spain). E-mail: carlosantonio.platero@upm.es

G. Navarro is with the Spanish Public Research Centre on Energy, Environment and Technology, CIEMAT, Ministerio de Innovación, Ciencia y Universidades, Madrid 28037 (Spain). E-mail: gustavo.navarro@ciemat.es

E. Neutral current injection device

This method needs to install a current source between a neutral connection of the power system and ground combined with a current sensor [24]. The current source can be a DC or AC current source (in case to be an AC source, the injection current must have different frequency from the operating system one). Afterward, if a ground fault occurs, the current injection system closes its circuit returning from the ground. At this moment, the measurement device detects the fault and notices it to the appropriate protection device.

F. Neutral voltage injector device

In this case, a voltage injector is placed in the same position as the current source explained above. It emits an AC voltage wave with different frequency than the operating one. Then, the current is measured in the same way as previously described. If a ground faults occurs, the current in the grounding resistor increase and an alarm is emitted when it exceeds the threshold [13], [25]. This equipment can be also used with the system off-line, for example in large synchronous stator diagnosis [14].

G. Statistical methods

In terms of statistical methods used to detect ground faults, there are methods that can locate ground faults by trial and error from previous experiences and records of relays' trips during operation at different load conditions, fault lengths or other factors [26]. Other methods contemplate the comparison between real time fault records and historical fault logs, as it can be the Laplace test statistic. These methods allow an online monitoring [27]. Finally, there exist methods that examine the covariance index of the actual operating conditions attending to historical ground fault locations to trip the protections and detect the failure [28].

TABLE I
STATE OF THE ART GROUND FAULT DIAGNOSIS POSSIBILITIES

Method and Reference		AC or DC detection	AC + DC detection	DC location	AC location
51 N	[17]	✓			
59 N	[18],[19]	✓			
	[20]	✓		✓	
87 N	[21],[22]	✓	✓		
21	[23]	✓			
Current Inj.	[24]	✓	✓		
Voltage Inj.	[13],[14]	✓		✓ ([13])	✓ ([14])
	[25]	✓	✓		
Statistical	[26]	✓			✓
	[27],[28]	✓			
Artificial Intelligence	[11],[29],[30]	✓			
	[12],[31]	✓		✓ ([12])	✓ ([31])
Ungrounded	[16]	✓			✓
	[32],[33]	✓			
Previous research	[34]	✓	✓		
Proposed					✓

H. Artificial intelligence methods

As in statistical methods, machine learning methods can be trained for ground fault detection inserting previous fault data. These methods can be trained for detection and classification of different type of faults, e.g., in photovoltaic systems [29], or in induction motors [30], among others. But also, they can be trained to detect and locate an specific type of fault in a determined system, for example, to locate ground faults in distributed systems [12],[31].

On the other hand, there also exist methods to detect ground fault in ungrounded systems. One example is [16], which uses the low voltage side measurements during a ground fault to locate the defect in distribution networks. For power converters, in [32] the IGBTs' voltage during the switching period is analyzed. With fault, the IGBT commutation is slower due to the arc resistance and its voltage will increase faster than in case of non-fault. To protect the DC side of DC-AC systems, electronic circuits could be coupled to each cell of the DC source. They actuate as a Battery Manage System (BMS) to detect ground faults [33].

For whole DC-AC systems, the ground fault diagnosis is a complex task. The difficulty resides in the ground fault location, i.e., in which point of the electric system it is located. Due to this problem, the installation of a grounding resistor between the midpoint of the DC bus and ground was proposed [34]. By measuring the voltage between its terminals, the discrimination between DC + pole, DC – pole and AC ground faults was achieved but its exact location still being incognita.

Table I collects the commented techniques and particular methods in order to sum up this section.

In this paper, an improvement of the previous method [34] is proposed. It consists of a location method for AC side ground faults for DC-AC systems. The method is also based in the installation of a grounding resistor connected between the midpoint of the DC bus and ground where its voltage is measured. Applying a histogram to this measurement allow the key parameters' estimation in order to get the ground fault location. This method was previously presented in its conference form in [35] where some computer simulations were presented. In this manuscript, the method is also validated through experimental results using a 140 kW power converter. Additionally, the method has granted a Spanish patent [36], and completes the discrimination method presented in [34] by locating the percentage of impedance where the fault is taking place.

The paper is structured as follow: Section II details the operation principles of the proposed ground fault location method. Then, Section III describes the simulation model and analyzes the computer simulations results, where Section IV shows the experimental results from the tests carried out in a 140 kW power inverter. Lastly, Section V concludes with the main contributions of the proposed method.

II. OPERATION PRINCIPLES OF THE GROUND FAULT LOCATION METHOD

In this section, the operation principles for the location of ground faults in the AC side of inverters are explained.

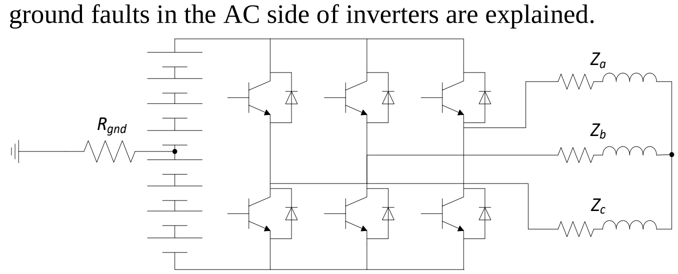

Fig. 1. Grounding resistor installed between the midpoint of the DC bus and

ground, in an AC load feed from batteries through a converter.

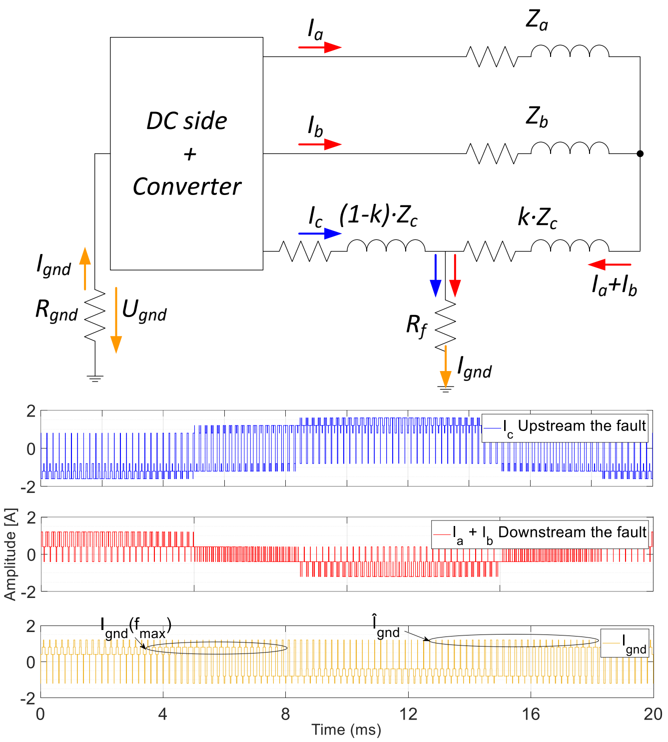

Fig. 2. AC side of a power converter with a ground fault in the phase "c". A grounding resistor, R_{gnd}, is installed in the midpoint of the DC bus. The DC bus and converter are collected in a black box [An example of upstream, downstream and faulty currents are displayed respectively for all impedances Z = 1+j0 Ω and 1 V – 50 Hz balanced PWM phase voltage waves].

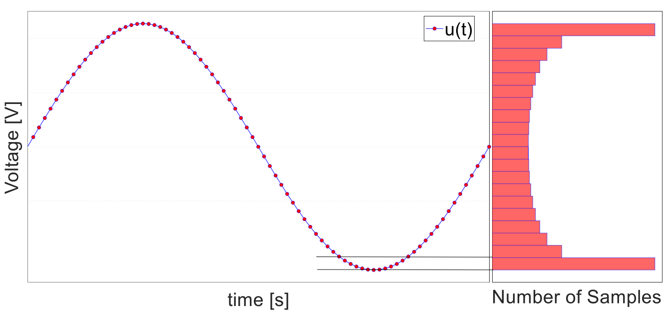

Fig. 3. Theoretical example of histogram carried out in a sinusoidal wave.

The most important factor for this method is to install a grounding resistor (R_{gnd}) between the midpoint of the DC bus of the power inverter and ground as seen in [34]. This configuration is also shown in the DC-AC system of Fig. 1, where R_{gnd} is connected in the midpoint of a battery pack. The battery feeds an RL load which emulates a steady state motor placed in the AC side of the inverter. This way, the fault current can be estimated by measuring the voltage in terminals of the grounding resistor, U_{gnd}.

In healthy conditions, there is no fault current and consequently U_{gnd} is null. However, if a ground fault occurs in the AC side, there is an AC fault current circulating through R_{gnd}, then, U_{gnd} will be different from zero and it will also have AC components.

In the AC side, the phase impedances can be or not balanced and the ground fault can have or not a fault resistance (R_f). For a generic case, the AC system is analyzed is as it is shown in Fig. 2. In this figure, an example of faulty situation is presented where the upstream (I_c), downstream ($I_a + I_b$) and faulty currents (I_{gnd}) are analyzed.

Two types of approaches will be analyzed. On one hand, an unbalanced system as the general method. On the other hand, the balanced system, as a particular case, which it is consider representative due to the large quantity of these systems and because of the simplification of the method. For this second scenery, all the impedances of Fig. 2 are Z = 1+j0 Ω and the phase voltages are balanced PWM waves of 1 V – 50 Hz.

A. *General AC system method approach*

If a ground fault occurs in the AC side of the inverter, one of the phases has a leakage current (e.g., in phase "c") and the grounding resistor placed in the midpoint of the DC bus will measure between its terminals a pulsed voltage wave (See Fig. 2). This pulsed wave is proportional to the leakage current if the fault is merely resistive and it has two main components, in which the method is based on:

1) *The most repeated voltage range, $U_{gnd}(f_{max})$*

The most repeated voltage range component measured in R_{gnd} is due to the addition of the currents that comes from the healthy phases in the downstream side of the fault (See $I_a + I_b$ in comparison with U_{gnd} in Fig. 2) through ground. This parameter is proportionally supported by the contribution of the two healthy phases' impedances, Z_a, and Z_b, and the downstream faulty phase impedance, $k{\cdot}Z_c$. This voltage component will have a higher number of samples than the one introduced by the faulty phase, because at least 4 IGBTs are involved in this faulty circuit, then the pulse width duty is higher.

2) *The greatest voltage range, $\hat{U}_{gnd}$*

The highest amplitude of the pulses can only be possible in certain moments, when the three phase currents are added ($I_a + I_b + I_c$) product of the imbalance provoked by the ground fault, i.e., all the upper or lower IGBTs of the converter are enable at the same time. It means that all the impedances support this component.

For this reason, a coefficient, called global fault coefficient, is defined as the division of the two components before (1).

$$C_S = \frac{U_{gnd}(f_{max})}{\hat{U}_{gnd}} \quad (1)$$

The global fault coefficient can be expressed by the use of the impedances instead of voltage components as in (2):

$$C_S = \frac{Z_a//Z_b + k{\cdot}Z_c}{Z_a//Z_b + k{\cdot}Z_c + (1-k){\cdot}Z_c} \quad (2)$$

where k is the length per unit of impedance where the fault is located ($k = 1$ in terminals of the AC side of the power inverter, and $k = 0$ in the neutral of the load).

Obtaining k from expression (2), the final expression (3) is achieved:

$$k = C_S + \frac{Z_a{\cdot}Z_b}{Z_c{\cdot}(Z_a+Z_b)} \cdot (C_S - 1) \quad (3)$$

This expression suggests that the system must be characterized before the application of the method. Then, in (3), it can be observed that the global fault coefficient would be the unique variable of the equation if the phase impedances are linear. Therefore, this method could be valid for ground fault diagnosis during steady state condition. In order to achieve the values that allows the calculation of the global fault coefficient

(U_{gnd} (f_{max}) and $\hat{U}_{gnd}$), a histogram in voltage values is performed, where the registered instantaneous values of U_{gnd} are classified in different intervals. Fig. 3 shows an example of histogram applied into a sinusoidal wave. In the histogram, the value of the wider pulses, U_{gnd} (f_{max}), should correspond to the peak with the maximum number of repetitions different from zero. Afterwards, the greatest voltage value, $\hat{U}_{gnd}$, will be measured in the histogram in a second peak of repetitions after passing U_{gnd} (f_{max}) peak. It must be taken into account that $\hat{U}_{gnd}$ cannot be higher than the half-voltage of the DC bus in order to avoid undesirable errors in the method. When both values are located, the global fault coefficient is calculated, and the value of k can be estimated.

B. Particular case, the balanced AC system approach

The balanced system is a particular case of the general method, but this configuration is the most common in the industrial systems and electrical drives. In these systems, the AC impedance, Z, is the same for each phase of the system, then, replacing Z_a, Z_b and Z_c per Z in (3), a new equation (4) is given as:

$$k = \frac{1}{2}(3 \cdot C_S - 1) \tag{4}$$

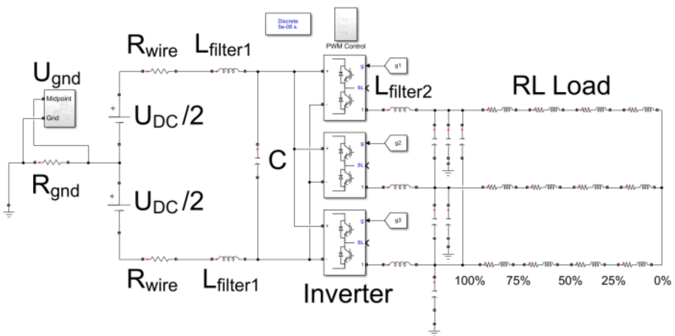

Fig. 4. Simulation model.

TABLE II
SIMULATION SETUP COMPONENTS

Component	Characteristic	Magnitude [a]
Grounding resistor	R	4700 Ω
Battery	U_{DC}	480 V
Cable resistance	R_{wire}	1 Ω
DC inductive filter	$L_{filter1}$	6 μH
Converter	C	1638 μF
	R_{int}	1 mΩ
	$R_{Snubber}$	1000 Ω
	$C_{Snubber}$	1 nF
AC inductive filter	$L_{filter2}$	3 mH
Inductive load (each fourth part)	R	12.5 Ω
	L	5 μH

As it can be seen in (4), a balanced system does not need the impedance characterization, simplifying considerably the ground fault location problem. In this particular case, only the grounding resistor voltage should be measured. Then, a histogram must be done in order to obtain the two components of C_S. Finally, the ground fault location is estimated, k. This way, the method complements the previous authors' technique [34], that it was only able to detect ground faults in DC-AC systems.

III. COMPUTER SIMULATIONS

In this section, numerous simulations have been carried out in a balanced system. For the simulations, a 480 V battery pack has been installed in the DC bus as well as a 1638 μF capacitor, which maintains the voltage in terminals of a three-phase power inverter. The battery is divided into two 240 V sources to have the midpoint accessible where a grounding resistor of 4.7 kΩ has been installed. Also, a RL load was installed in terminals of the AC side of the converter. The impedances values are $50 + j\omega 2\times10^{-5}$ Ω divided in four equal stages of $12.5 + j\omega 5\times10^{-6}$ Ω. This configuration allows to make ground faults in different parts of the load. The ground fault positions considered are 0% (neutral of the load), 25%, 50%, 75% and 100% (connection between the AC inverter and the load). Finally, some cable resistances and inductive filters are placed in the DC and AC sides of the power converter as well as some mutual and to-ground parasitic capacitances in order to get more realistic results. The complete system can be seen in Fig. 4 and its electrical parameters are presented in Table II.

Firstly, a healthy condition simulation was run, registering U_{gnd} during 40 ms simulation time (see Fig. 5), and calculating its corresponding histogram, that is shown in Fig. 6. In this figure it can be seen that no $U_{gnd}(f_{max})$ nether $\hat{U}_{gnd}$ parameters are detected as they are negligible.

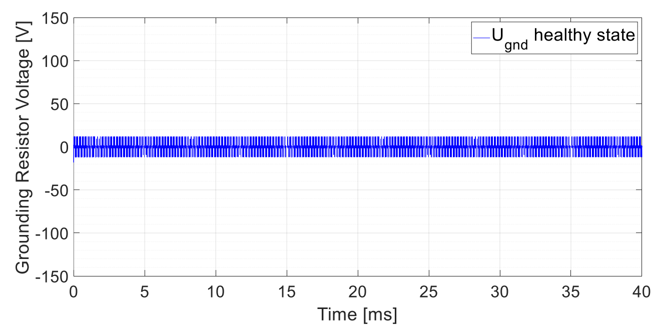

Fig. 5. Simulation measurement of the grounding resistor voltage during a healthy condition operation.

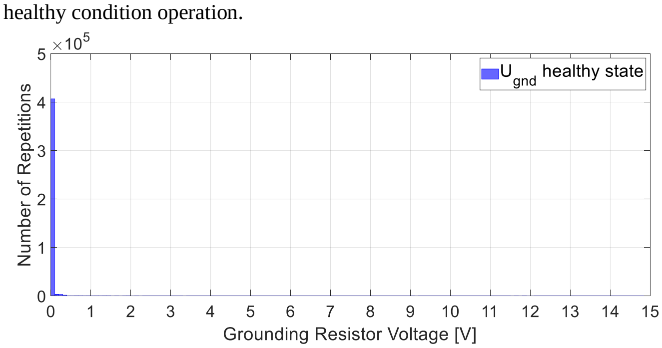

Fig. 6. Histogram for a 40 ms record of grounding resistor voltage wave. Healthy conditions.

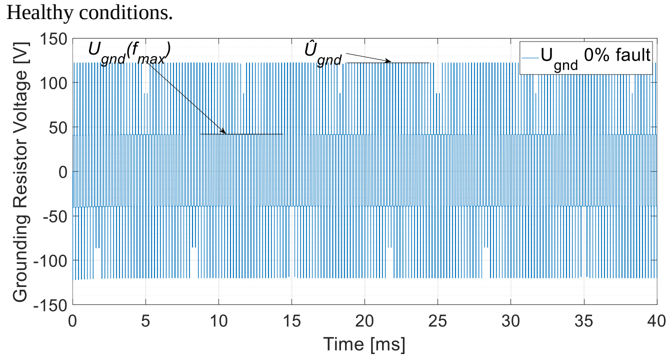

(a)

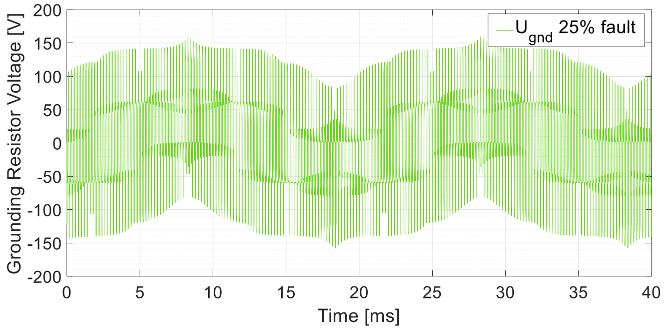

(b)

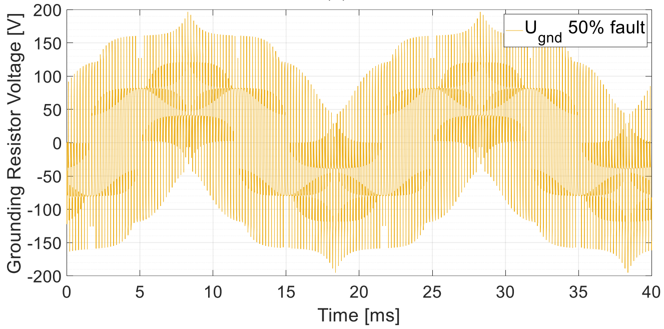

(c)

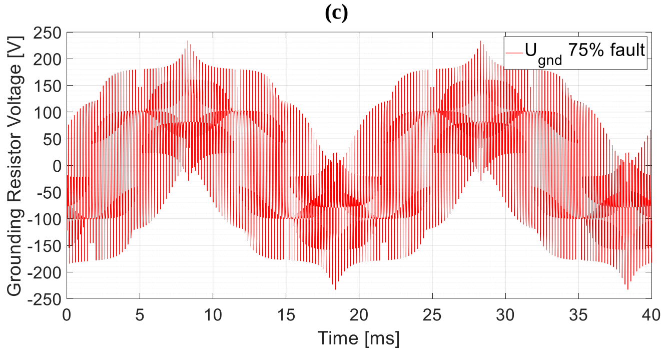

(d)

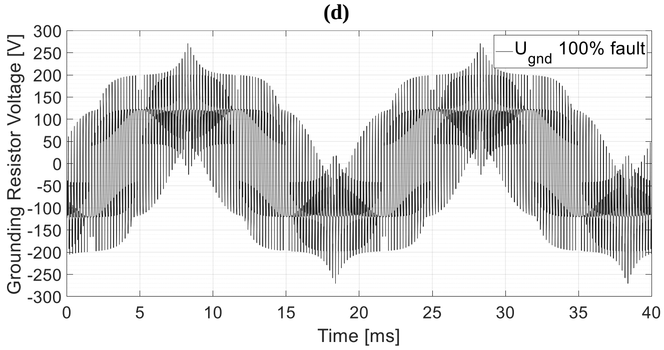

(e)

Fig. 7. Simulation of different ground faults with R_f = 4.7 kΩ: Grounding resistor voltage instantaneous measurements [AC impedance positions: (a): *k* = 0; (b): *k* = 25 %; (c): *k* = 50 %; (d): *k* = 75 %; (e): *k* = 100 %].

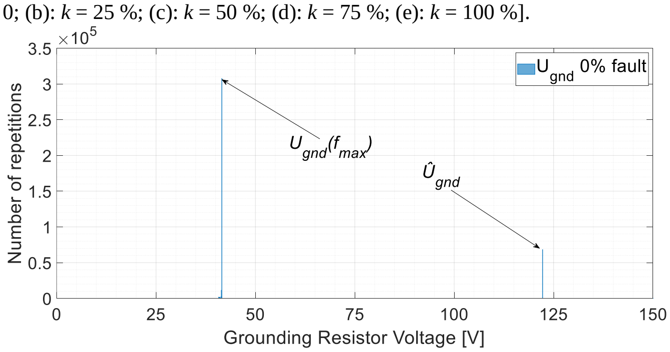

(a)

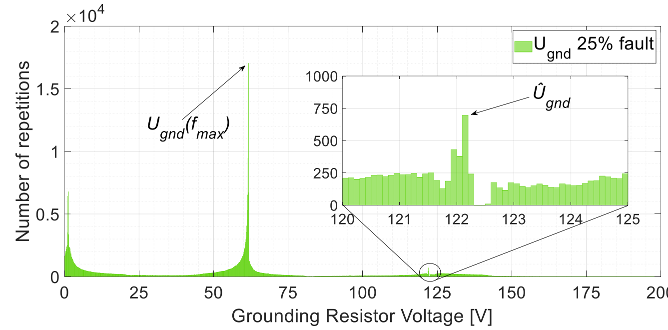

(b)

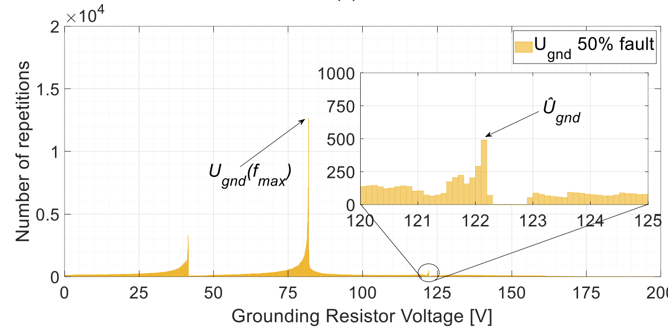

(c)

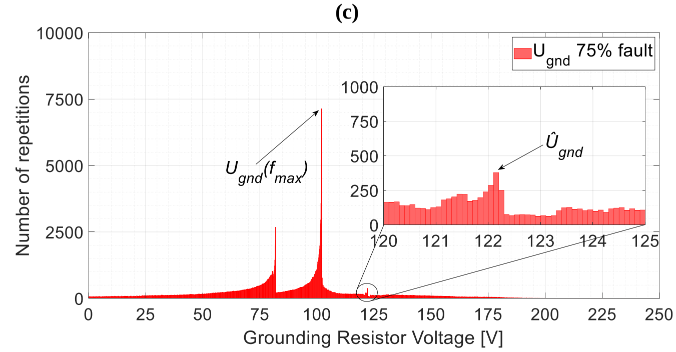

(d)

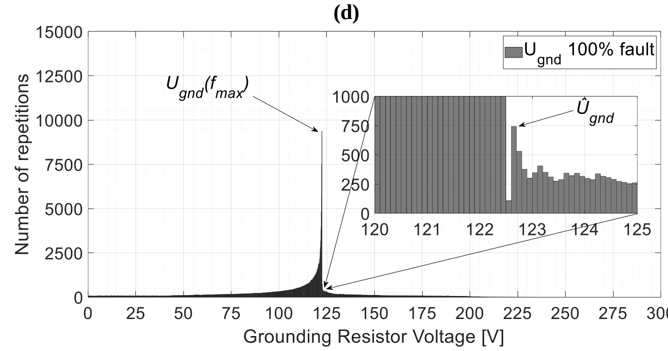

(e)

Fig. 8. Simulation of different ground faults with R_f = 4.7 kΩ: Grounding resistor voltage histograms for 40 ms wave records [AC impedance positions: (a): *k* = 0 %; (b): *k* = 25 %; (c): *k* = 50 %; (d): *k* = 75 %; (e): *k* = 100 %].

Afterward, numerous ground faults were performed. To validate the location method different simulations were performed with a 4.7 kΩ fault resistance at 0%, 25%, 50%, 75% and 100% of the impedance of the phase "c". The results of grounding resistor voltage waveforms are in Fig. 7.a to Fig. 7.e respectively. Then, when the wave is registered, U_{gnd} is different from zero and presents AC component, a histogram is performed to obtain the values of $U_{gnd}(f_{max})$ and $\hat{U}_{gnd}$. The range of values of the histogram must be chosen according to the calculation speed of the algorithm. In this simulations, 0.1 V intervals have been considered. Once the histogram is finished, some peaks are detected according to the voltage waveform (see

Fig. 8). These peaks are the maximum number of repetitions, $U_{gnd}(f_{max})$, which conforms the numerator of C_S, and the next peak registered past this first one, which is $\hat{U}_{gnd}$. The histograms' results are displayed in Fig. 8.a to Fig. 8.e for faults in k = 0%, 25%, 50%, 75% and 100% of the phase impedance respectively. Finally, the numerical values of $U_{gnd}(f_{max})$ and $\hat{U}_{gnd}$ are collected in Table III.

Furthermore, different ground faults with higher or lower R_f can occur. As the method do not take R_f into consideration, similar results may be achieved. To corroborate it, an additional simulation was accomplished with R_f = 100 Ω at k = 50 % of impedance in phase "c" in Fig. 9. As it can be seen, U_{gnd} amplitude is affected by R_f variations, being the voltage drop accentuated in R_{gnd}. Then, the higher R_f, the lower U_{gnd}. Additionally, the histogram for this fault is performed in Fig. 10 from the record of Fig. 9. In this figure, the most repeated voltage value corresponds to $U_{gnd}(f_{max})$ = 160.2 V and the greatest value peak is $\hat{U}_{gnd}$ = 239.2 V. Calculating C_S from (1) and applying (4), the location result for a ground fault in 50 % is 50.4599 %.

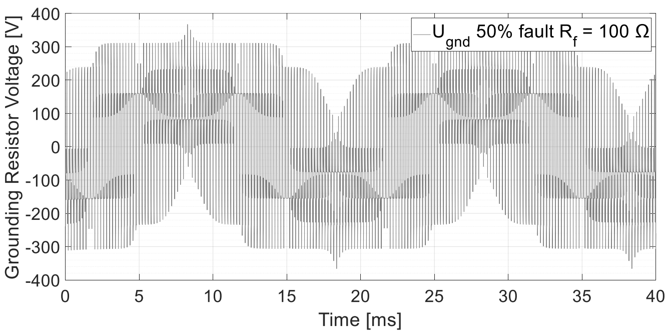

Fig. 9. Simulation of a ground fault in k = 50 % of the AC phase impedance with R_f = 100 Ω: Grounding resistor voltage instant measures.

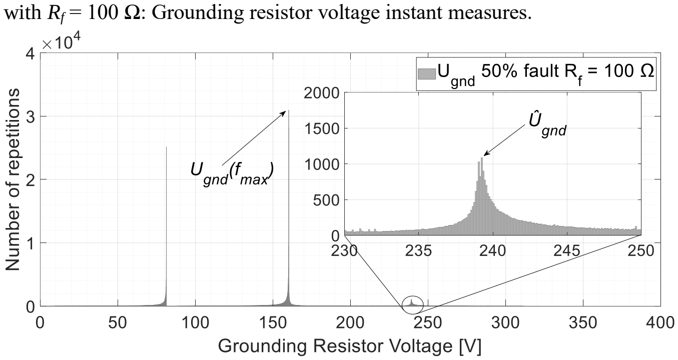

Fig. 10. Simulation of a ground fault in k = 0.50 of the AC phase impedance with R_f = 100 Ω: Histogram for 40 ms record of U_{gnd}.

TABLE III
SIMULATION RESULTS

Real ground fault location	$U_{gnd}(f_{max})$ [V]	$\hat{U}_{gnd}$ [V]	C_S	Estimated ground fault location
0 %	41.5	122.2	0.3396	0.94 %
25 %	61.6	122.1	0.5045	25.67 %
50 %	81.8	122.1	0.6699	50.49 %
75 %	102	122.1	0.8353	75.30 %
100 %	122.4	122.6	0.9983	99.75 %

As it can be seen, the method responds correctly to the ground faults simulations. On them, the error in the determination of the ground fault location is around ±1 %. Additionally, the method does not depend on the ground fault resistance, and if the AC system is balanced, nether the AC impedance is needed.

IV. EXPERIMENTAL RESULTS

To support the simulation results, some experimental tests were carried out in a 140 kW power inverter. The experimental tests were performed in healthy state, (with no ground fault) and with R_f = 0 Ω, 2.3 kΩ, 4.7 kΩ and 10 kΩ at different locations of the load in the AC side of the inverter.

A. *Experimental setup characteristics*

The DC/AC system of the experimental setup consists of a 140 kW power converter connected to a three phase resistor in the AC side that are fed from 480 V_{DC} batteries in the DC side.

The power inverter is operated as a voltage source converter (VSC). In the DC side of the inverter a capacitor of 1638 μF is connected and in the AC side terminals there are installed 3 mH inductive filters to each phase. Fig. 11 shows a cabinet with the power inverter.

On the AC side of the system, a three-phase resistive load is connected (see Fig. 12). The phase impedances have a value of 50 Ω and they are composed of four power resistances of 12.5 Ω each connected in series. This allows the introduction of fault resistances at different locations. In Fig. 12, there is also a switch to perform ground faults in the different positions of one of the three phases. The location of theses faults are k = 0%, 25%, 50%, 75% and 100% of the impedance, where 0% corresponds to the neutral of the load and 100% is the terminal of the inverter.

On the DC side, the batteries feed the electric system. They are composed by 40 modules of 12 V_{DC} each with all the cells placed in series. This provides to the system a voltage of 480 V_{DC}. The batteries cabinet can be seen in Fig. 13 as well as its protections and maneuver devices.

As the batteries have 40 modules connected in series, a grounding resistor of R_{gnd} = 4.7 kΩ should be connected from the 20th module to ground. This connection corresponds to the midpoint of the battery pack. The voltage between the energized midpoint terminal and ground is 0 V in case of healthy operation. The grounding resistor limits the fault current to 51 mA in case of a ground fault with R_f = 0 Ω at the negative or positive terminals.

In order to sum up the experimental setup, the whole system characteristics are compiled in Table IV.

Fig. 11. 140 kW power inverter.

Fig. 12. Resistive load [R_{phase} = 50 Ω].

Fig. 13. 480 V Battery pack [1 string of 40 modules of 12 V_{DC} each].

B. *Experimental tests.*

Once the system has been installed, a healthy operation test is carried out to check that the system runs correctly. Fig. 14 shows that the voltage in the grounding resistor is around 0 V. The high frequency noises are provoked by the parasitic capacitances to ground. It can be clearly seen that there are not ground faults in the system because once the histogram is done, there are not representative peaks (see Fig. 15). Then, if a high number of samples appear near to 0 V in the histogram, it will imply the correct operation of the DC-AC system.

TABLE IV
EXPERIMENTAL SETUP CHARACTERISTICS

Component	Characteristic	Magnitude
Battery	U_{DC}	480 V
	U_{DC} per cell	12 V/cell
	Modules per String	40
	I_N	3.6 A
	Q	12 Ah
	Internal R	12 mΩ
Inverter	P_N	140 kW
	U_{DC} max.	900 V
	I_{out} max.	200 A
	f max.	25 kHz
	C	1.638 mF
	L_{filter}	3 mH
Resistor	R_{unit}	12.5 Ω
	R_{phase}	50 Ω
	P_{unit}	392 W
	Total Three-phase Power	4704 W

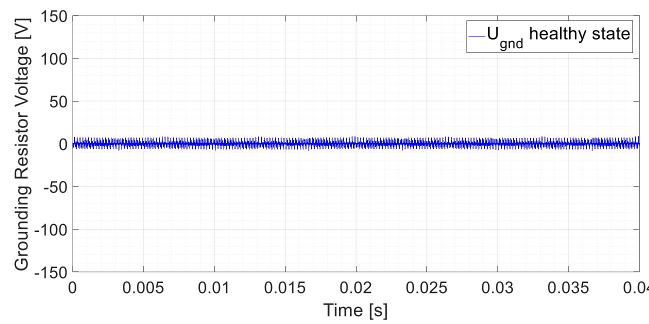

Fig. 14. Grounding resistor voltage for a healthy state test.

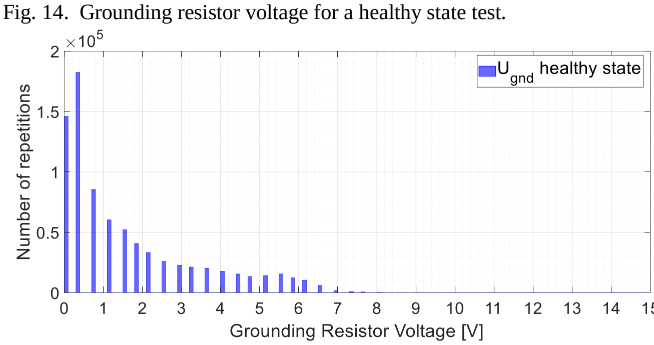

Fig. 15. Grounding resistor voltage histogram for a 40 ms register of healthy state operation.

After a healthy state test was carried out, some ground faults at different locations were accomplished. The tests were performed varying the location of the fault between k = 0%, 25%, 50%, 75% and 100% of the impedance for different fault resistances (R_f = 0 Ω, 2.3 kΩ, 4.7 kΩ and 10 kΩ).

In the faulty tests, a grounding resistor voltage appears in R_{gnd}. It is produced due to the fault current circulation. If the fault is located in the AC side, U_{gnd} has AC components. It can be observed in the different 40 ms records taken from faults of 4.7 kΩ in locations of 0%, 25%, 50%, 75% and 100% plotted from Fig. 16.a to Fig. 16.e, respectively. It can be seen how the waveform varies from the neutral (k = 0%) to terminals of the power inverter (k = 100%). Also, the voltage magnitude decreases when the fault is near to the neutral of the AC load.

Once having the waves' registers, a histogram is done. In this case, for 40 ms, 10^6 instant values have been collected and ordered by intervals of 0.1 V from 0 V up to 250 V. The results are shown from Fig. 17.a to Fig. 17.e, for the previous fault locations, respectively.

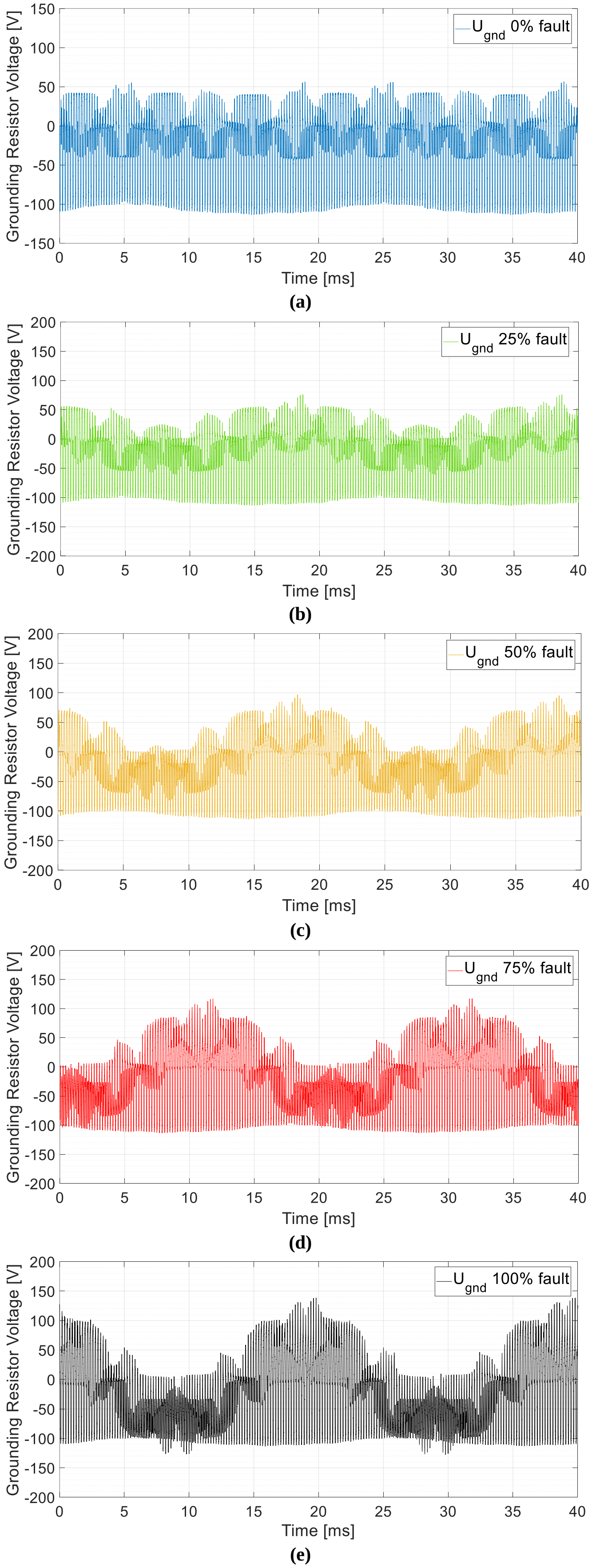

Fig. 16. Experimental results of different ground faults with $R_f = 4.7$ kΩ: U_{gnd} instantaneous measurements [AC impedance positions: (a): $k = 0$; (b): $k = 25$ %; (c): $k = 50$ %; (d): $k = 75$ %; (e): $k = 100$ %].

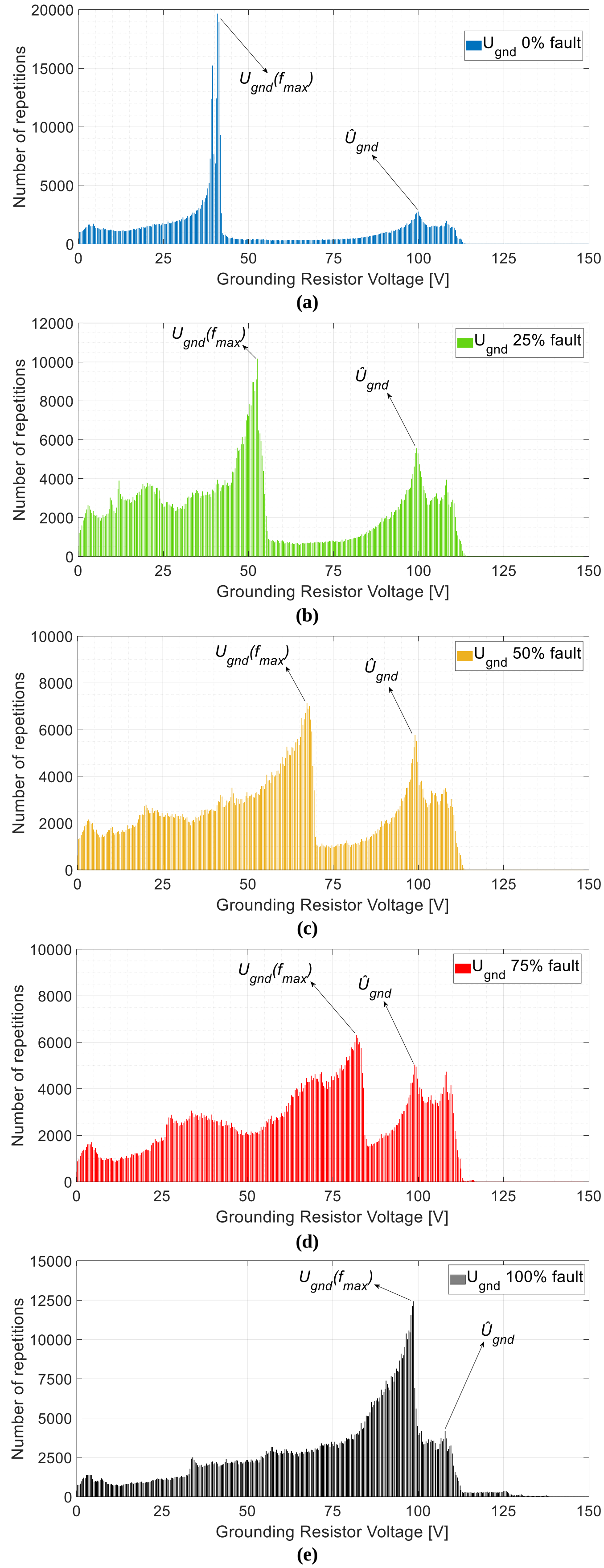

Fig. 17. Experimental results of different ground faults with $R_f = 4.7$ kΩ: U_{gnd} histograms for 40 ms wave records [AC impedance positions: (a): $k = 0$ %; (b): $k = 25$ %; (c): $k = 50$ %; (d): $k = 75$ %; (e): $k = 100$ %].

TABLE V
EXPERIMENTAL RESULTS

Real ground fault location	$U_{gnd}(f_{max})$ [V]	$\hat{U}_{gnd}$ [V]	C_S	Estimated ground fault location
		$R_f = 0\ \Omega$		
0 %	83.3 V	194.5 V	0.4283	14.24%
25 %	107.9 V	194.1 V	0.5559	33.38%
50 %	137.5 V	192.7 V	0.7135	57.03%
75 %	166.7 V	191.6 V	0.8700	80.51%
100 %	190.1 V	211.7 V	0.8980	84.70%
		$R_f = 2.3$ kΩ		
0 %	57.0 V	136.0 V	0.4191	12.87%
25 %	73.8 V	135.6 V	0.5442	31.64%
50 %	95.0 V	134.6 V	0.7058	55.87%
75 %	114 V	134.9 V	0.8451	76.76%
100 %	134.6 V	145.5 V	0.9251	88.76%
		$R_f = 4.7$ kΩ		
0 %	40.9 V	99.8 V	0.4098	11.47%
25 %	53.0 V	99.4 V	0.5332	29.98%
50 %	67.3 V	99.0 V	0.6798	51.97%
75 %	81.9 V	99.0 V	0.8273	74.09%
100 %	98.7 V	107.9 V	0.9147	87.21%
		$R_f = 10$ kΩ		
0 %	26.3 V	65.4 V	0.4021	10.32%
25 %	33.6 V	65.4 V	0.5138	27.06%
50 %	43.5 V	65.4 V	0.6651	49.77%
75 %	52.6 V	64.6 V	0.8142	72.14%
100 %	64.6 V	70.5 V	0.9163	87.45%

Some peaks can be observed in the histograms. There are two important peaks to highlight. The first one is the clearly seen in Fig. 17.a to Fig. 17.d as the most repeated peak. This value, U_{gnd} (f_{max}), becomes displaced to higher voltages and also attenuated as nearer is the fault location from the power inverter terminals ($k \rightarrow 1$). The other peak is located after the valley provoked by the U_{gnd} (f_{max}) peak, which is the greatest voltage value, $\hat{U}_{gnd}$. With both peaks, C_S can be calculated and (4) can be carried out obtaining the fault location, k.

One problem is presented in Fig. 17.e, where the peaks are not as distinguishable as in the cases before because they are superposed. In this case, the method's algorithm will choose the following peak, provoking an estimation error. In this field, the method is more accurate for faults near to the neutral of the load than for faults near to the inverter's terminals. However, if the global fault coefficient, C_S (1) is calculated with the wrong values (case $k = 1$), the method estimates a not far away location for the ground fault.

For faults with different R_f ($R_f = 0$, see Fig. 18 and Fig. 19), U_{gnd} amplitude increases considerably compared with $R_f = 4.7$ kΩ tests, as all the voltage drop is considered in R_{gnd}. However, in the histogram carried out in Fig. 19, the proportion between peaks is nearly the same as for other faults performed in the same location ($k = 50$ %) with different R_f. This means they have the same C_S and consequently, the same k estimation.

As it can be observed in Table V, the method gives an accurate estimation of the fault position. The errors are quite small when the ground fault location is closed to the midpoint of the load impedance. The best estimation has an absolute error of 0.23 %. However, if the fault is near to the terminals of the power inverter and the fault resistance is low, the accuracy of the method decreases remarkably. In these conditions the errors can reach 15.30 %.

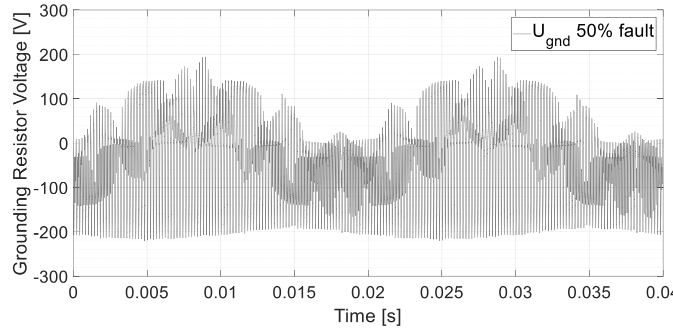

Fig. 18. Grounding resistor voltage waveform for a 40 ms register of a 0 Ω fault in 50 % of the phase impedance.

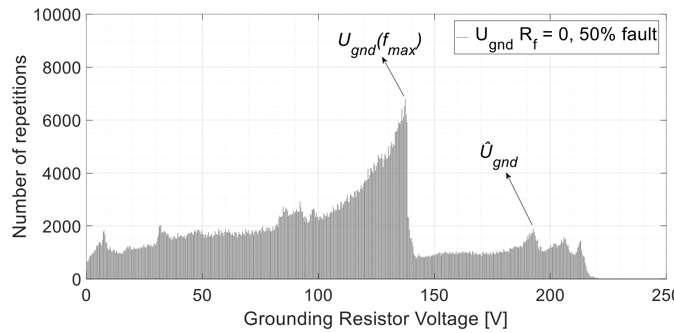

Fig. 19. Grounding resistor voltage histogram for a 40 ms register of a 0 Ω fault in 50 % of the phase impedance.

The experimental tests do not give results as accurate as those obtained in the computer simulations. But measuring only in terminals of R_{gnd}, an estimation of AC ground fault location in DC/AC systems could be achieve.

V. CONCLUSION

In this paper, a new location method of AC ground faults in DC/AC inverters was presented. It is based on the measurement of the voltage wave in a grounding resistor connected between the midpoint of the DC bus and ground in case of ground fault. Then, with this voltage record, a histogram is performed using small intervals to calculate two correlated parameters, the most repetitive voltage range and the greatest voltage range value. With these two factors, a global fault coefficient is calculated. Afterward, the fault location can be estimated and expressed in percentage of the position, 0 % corresponds to the neutral of the load and 100% to the inverter terminal. In case of an unbalance system, with different impedances per phase, the values of these impedances are required for the estimation. However, in case of a balance system the value of the load impedance is not required.

To prove and corroborate the theoretical principles where the method is based on, a huge number of simulations have been performed. The simulations results were satisfactory, achieving estimation errors of the fault location around 1%. Also, experimental tests have been carried out for several ground fault locations with different fault resistances. The experimental results are not so satisfactory, as the location errors increase up to 15%.

It was observed that the most repeated voltage range becomes attenuated when the faults is near to the AC terminals of the inverter. In the experimental setup, inherent asymmetries and other factors not considered in the simulation model should be deeper investigated in future research to improve the accuracy of the proposed method. Additionally, all future investigation in this research line should use SiC transistors, as they will replace IGBTs as commutation elements for AC drives.

Despite of this, the main advantages of the proposed method are that the fault resistance or load impedance values are not needed, it is simple to be installed and it gives an estimation of the position just by the analysis of a record of the voltage wave in the grounding resistor.

Acknowledgment

Authors would like to acknowledge Mr. Lafoz for his implication in this work.

References

[1] S. Yang. A. Bryant. P. Mawby. D. Xiang. L. Ran and P. Tavner. "An Industry-Based Survey of Reliability in Power Electronic Converters." *in IEEE Transactions on Industry Applications*. vol. 47. no. 3. pp. 1441-1451. May-June 2011.

[2] R. Li and F. Shi. "Control and Optimization of Residential Photovoltaic Power Generation System With High Efficiency Isolated Bidirectional DC–DC Converter." *in IEEE Access*. vol. 7. pp. 116107-116122. 2019.

[3] A. Renault. J. Rodas. L. Comparatore. J. Pacher and R. Gregor. "Modulated Predictive Current Control Technique for a Three-Phase Four-Wire Active Power Filter based on H-bridge Two-Level Converter." *2018 53rd International Universities Power Engineering Conference (UPEC)*. Glasgow. 2018. pp. 1-6.

[4] D. Caballero et al. "Predictive Voltage Control using Matrix Converter for a Stand-alone Wind Energy based Microgrid." *2018 IEEE International Conference on Automation/XXIII Congress of the Chilean Association of Automatic Control (ICA-ACCA)*. Concepcion. 2018. pp. 1-6.

[5] T. Ahonen. R. Tiainen . J. Viholainen. J. Ahola and J. Kestila. "Pump operation monitoring applying frequency converter." *2008 International Symposium on Power Electronics. Electrical Drives. Automation and Motion*. Ischia. 2008. pp. 184-189.

[6] L. Yang. W. Zhang. X. Zhang and G. P. Li. "Nonlinear variable frequency control of high power switched-capacitor converter." *2016 IEEE 8th International Power Electronics and Motion Control Conference (IPEMC-ECCE Asia)*. Hefei. 2016. pp. 3472-3476.

[7] N. Weise. "DQ current control of a bidirectional. isolated. single-stage AC-DC converter for vehicle-to-grid applications." *2013 IEEE Power & Energy Society General Meeting*. Vancouver. BC. 2013. pp. 1-5.

[8] A. Wangsupphaphol. N. R. N. Idris. A. Jusoh. N. D. Muhamad and I. M. Alsofyani. "Acceleration-based design auxiliary power source for Electric Vehicle applications." *2014 11th International Conference on Electrical Engineering/Electronics. Computer. Telecommunications and Information Technology (ECTI-CON)*. Nakhon Ratchasima. 2014. pp. 1-6.

[9] A. Mohamed. S. Vanteddu and O. Mohammed. "Protection of bi-directional AC-DC/DC-AC converter in hybrid AC/DC microgrids." *2012 Proceedings of IEEE Southeastcon*. Orlando. FL. 2012. pp. 1-6.

[10] B. Li, W. Wang, B. Li, Y. Liu, W. Wen, X. Chen, "Research on a current calculation method and characteristics of pole-to-ground faults in true bipolar MMC-HVDC grids considering line coupling," *Electric Power Systems Research*, Volume 192, 2021, 106985.

[11] K. Moloi and A. A. Yusuff, "Power Distribution System Fault Diagnostic Using Genetic Algorithm and Neural Network," *2021 Southern African Universities Power Engineering Conference/Robotics and Mechatronics/Pattern Recognition Association of South Africa (SAUPEC/RobMech/PRASA)*, 2021, pp. 1-5.

[12] Y. Pan. M. Steurer and T. L. Baldwin. "Ground Fault Location Testing of a Noise-Pattern-Based Approach on an Ungrounded DC System." *in IEEE Transactions on Industry Applications*. vol. 47. no. 2. pp. 996-1002. March-April 2011.

[13] J. Park. "Ground Fault Detection and Location for Ungrounded DC Traction Power Systems." *in IEEE Transactions on Vehicular Technology*. vol. 64. no. 12. pp. 5667-5676. Dec. 2015.

[14] M. Davarpanah et al.. "Precise Locating of Stator Winding Earth Fault in Large Synchronous Generators." *in IEEE Transactions on Industry Applications*. vol. 53. no. 3. pp. 3137-3145. May-June 2017.

[15] C. A. P. Gaona. F. Blázquez. P. Frías and M. Redondo. "A Novel Rotor Ground-Fault-Detection Technique for Synchronous Machines With Static Excitation." *in IEEE Transactions on Energy Conversion*. vol. 25. no. 4. pp. 965-973. Dec. 2010.

[16] K. Jia. Z. Ren. T. Bi and Q. Yang. "Ground Fault Location Using the Low-Voltage-Side Recorded Data in Distribution Systems." *in IEEE Transactions on Industry Applications*. vol. 51. no. 6. pp. 4994-5001. Nov.-Dec. 2015.

[17] S. R. Madeti, S. N. Singh. "A comprehensive study on different types of faults and detection techniques for solar photovoltaic system." *Solar Energy*. vol. 158, pp. 161-185, 2017.

[18] C. A. Platero. M. Redondo. M. Pardo and E. Rebollo. "Novel adaptive 100% stator ground fault protection based on the third harmonic measurement." *2016 XXII International Conference on Electrical Machines (ICEM)*. Lausanne. 2016. pp. 2300-2305.

[19] S. Turner. "Applying 100% stator ground fault protection by low frequency injection for generators." *2009 IEEE Power & Energy Society General Meeting*. Calgary. AB. 2009. pp. 1-6.

[20] F. R. Blánquez, M. Aranda, E. Rebollo, F. Blázquez and C. A. Platero, "New Fault-Resistance Estimation Algorithm for Rotor-Winding Ground-Fault Online Location in Synchronous Machines With Static Excitation," in *IEEE Transactions on Industrial Electronics*, vol. 62, no. 3, pp. 1901-1911, March 2015.

[21] Arc fault detector. by R. Mernyk and R. Bradley (2005 Jul. 14). W.O. Patent No. 2005/062917 A2.

[22] T. Gruhn, J. Glenney and M. Savostianik, "Type B Ground-Fault Protection on Adjustable Frequency Drives," in *IEEE Transactions on Industry Applications*, vol. 54, no. 1, pp. 934-939, Jan.-Feb. 2018.

[23] Method and adaptative distance protection relay for power transmission lines. by M. Saha. E. Roslowski and J. Izykowski (2011. Jan. 18). U.S. Patent No. 7.872.478.

[24] Y. Liu, E. Chang, Y. Lee, Y. Lin, "Detection of Ground Insulation Faults in Ungrounded DC Power Supply Systems by Using a DC Current Injection Method." *Energy Procedia*. vol. 156, pp. 349-355, 2019.

[25] C. Sun et al.. "High Frequency Voltage Injection based Fault Detection of Rotating Rectifier for Three-stage Synchronous Starter/Generator in the Stationary State." *2019 IEEE Applied Power Electronics Conference and Exposition (APEC)*. Anaheim. CA. USA. 2019. pp. 1024-1028.

[26] H. Chunfang. Z. Gecheng. C. Daifeng and C. Bo. "Probabilistic single line-ground fault location in non-effective grounded system." *2010 IEEE 11th International Conference on Probabilistic Methods Applied to Power Systems*. Singapore. 2010. pp. 271-276.

[27] C. J. Kim, S.Lee and S. Kang, "Evaluation of feeder monitoring parameters for incipient fault detection using Laplace trend statistic." *in IEEE Transactions on Industry Applications.* vol. 40. no. 6. pp. 1718-1724. Nov.-Dec. 2004.

[28] Z. Shi. S. Liu. S. Wang and Y. Liu. "Synchrophasors Covariance Index-based Fault Section Location for Active Distribution Networks." *2019 14th IEEE Conference on Industrial Electronics and Applications (ICIEA).* Xi'an. China. 2019. pp. 1703-1707.

[29] A. Eskandari, J. Milimonfared and M. Aghaei, "Fault Detection and Classification for Photovoltaic Systems Based on Hierarchical Classification and Machine Learning Technique," in *IEEE Transactions on Industrial Electronics*, vol. 68, no. 12, pp. 12750-12759, Dec. 2021.

[30] M. Z. Ali, M. N. S. K. Shabbir, S. M. K. Zaman and X. Liang, "Single- and Multi-Fault Diagnosis Using Machine Learning for Variable Frequency Drive-Fed Induction Motors," in *IEEE Transactions on Industry Applications*, vol. 56, no. 3, pp. 2324-2337, May-June 2020.

[31] H. Mirshekali, R. Dashti, H. R. Shaker, R. Samsami and A. J. Torabi, "Linear and Nonlinear Fault Location in Smart Distribution Network Under Line Parameter Uncertainty," in *IEEE Transactions on Industrial Informatics*, vol. 17, no. 12, pp. 8308-8318, Dec. 2021.

[32] M. A. Rodríguez-Blanco, A. Vázquez-Pérez, L. Hernández-González, V. Golikov, J. Aguayo-Alquicira and M. May-Alarcón, "Fault Detection for IGBT Using Adaptive Thresholds During the Turn-on Transient," in *IEEE Transactions on Industrial Electronics*, vol. 62, no. 3, pp. 1975-1983, March 2015.

[33] F. Saidani, F.X. Hutter, W. Selinger, S. Rößler, W. Braunwarth, J.N. Burghartz, "An integrated electronic circuit for decentralized monitoring of Lithium-ion battery cells", *MikroSystem Technik Kongress*, 2017, pp. 566-569, 2017.

[34] J. M. Guerrero, G. Navarro, C. A. Platero, P. Tian and F. Blázquez, "A Novel Ground Fault Detection Method for Electric Vehicle Powertrains

Based on a Grounding Resistor Voltage Analysis," in *IEEE Transactions on Industry Applications*, vol. 56, no. 5, pp. 4934-4944, Sept.-Oct. 2020.
[35] J. M. Guerrero, G. Navarro and C. A. Platero, "AC Ground Fault Location for DC-AC systems based on a Grounding Resistor Voltage Analysis," *2020 IEEE International Conference on Environment and Electrical Engineering and 2020 IEEE Industrial and Commercial Power Systems Europe (EEEIC / I&CPS Europe)*, Madrid, Spain, 2020, pp. 1-6.
[36] J. M. Guerrero and C. A. Platero “Sistema y Método de Localización de Faltas a Tierra en Corriente Alterna en Sistemas de Corriente Continua con Inversores”. Spanish Patent ES 2736412 B2. (2020, June 3).

AUTHORS’ INFORMATION

José Manuel Guerrero was born in 1996 in Madrid. Spain. He obtained his Bachelor degree in Energy Resources. Fuels and Explosive Engineering from the Universidad Politécnica of Madrid. Spain. in 2018. He received his Master degree in Electrical Engineering from Universidad Politécnica de Madrid (Spain) in 2019.

He works as Assistant Professor in the Energy and Fuels’ Department at the Universidad Politécnica of Madrid.

Gustavo Navarro was born in 1982 in Madrid. Spain. He received his degree in electronic engineering from the Universidad Politécnica de Madrid. Spain. in 2007.

Since 2007 he has been working as a research engineer in the Electrical Engineering Group at CIEMAT (Spanish Public Research Centre on Energy. Environment and Technology). His topics of interest are electrical drives control. energy storage systems (batteries and supercapacitors) and power electronics hardware design and validation.

Carlos A. Platero (M’10). (SM’20) was born in Madrid. Spain. in 1972. He obtained his Dipl. degree and Ph.D. degree in Electrical Engineering from the Universidad Politécnica de Madrid. Spain. in 1996 and 2007, respectively.

From 1996 to 2008 he worked in ABB Generación S.A. Alstom Power S.A. and ENDESA Generación SA. and was involved in the design and commissioning of power plants.

In 2002 he started teaching at the Electrical Engineering Department of the Universidad Politécnica de Madrid. and joined an energy research group. In 2008 he became a full-time Associate Professor.